Analysis of Yield Threshold in a Functionally Graded Variable Thickness Rotating Disc Using the Tresca Yield Criterion

sina khoonbani * and Hassan Ramezanian

Posted Date: 12 January 2024

doi: 10.20944/preprints202401.1020.v1

Keywords: Yield Threshold; Variable Thickness; Rotating Disk; Tresca Criterion; Yield Stress; Plastic Flow

Article

Analysis of Yield Threshold in a Functionally Graded Variable Thickness Rotating Disc Using the Tresca Yield Criterion

Sina Khoonbani * and Hasan Ramezanian

Department of mechanical Engineering , Amirkabir University of technology (Tehran polytechnic), Tehran, Iran
* Correspondence: khoonbani@aut.ac.ir

Abstract: The present article investigates the threshold analysis of yielding in a variable thickness rotating disk based on the Tresca criterion. The analysis is conducted on a Functionally Graded Material (FGM) constructed from tailored materials, following the theory of small deformations and for the case of plane stress. The elasticity modulus, density, and yield stress are assumed to be power functions of the radial coordinate. Poisson's ratio is considered constant due to small variations in different materials. Additionally, the governing equation for the rotating disk is solved analytically. Besides the material type, another factor affecting the distribution of effective stress magnitudes is the cross-sectional shape (profile) of the disk. The thickness of the cross-sectional disk varies radially as a power function. In the current analysis, different conditions for the onset of yielding and the evolution of plastic flow are considered. For evaluation and validation, the obtained results are compared and validated against similar results for specific cases (homogeneous disk and constant thickness graded disk) available in previous references. The results indicate that considering variable thickness for the disk section significantly affects the stresses and the location of the initiation of yielding.

Keywords: yield threshold; variable thickness; rotating disk; tresca criterion; yield stress; plastic flow

1. Introduccian

The rapid industrial advancement [1–6] in recent years has increased the human need for materials with optimal properties and special capabilities [7–15]. One category of new materials developed by scientists in this field is Functionally Graded Materials (FGM). FGM are composite materials that exhibit gradual and continuous variations in composition, structure, and properties in different directions within the component. The concept of Functionally Graded Materials was first introduced in 1984 [16] , and since then, research has continued to develop materials with high efficiency and heat resistance using the technology of gradual changes.

Rotating equipment plays a crucial role as one of the main components in various industries [17–21]. The industry of rotating equipment requires research and investigation in different areas due to its strategic role in various industries and the numerous parameters that significantly affect the performance and efficiency of the industrial processes.

Among the rotating components that have widespread applications and play a vital role is the rotating disc. The increasing use of rotating discs in diverse industries such as Power Generation Industry and Turbine Manufacturing, automotive [13,22–29], maritime, and others highlights its crucial importance in the industry [30–35].

Considering the significance of rotating discs in various industries, the analysis of these discs under different loading conditions becomes essential. Therefore, this research aims to provide a proper analysis to study the yielding behavior of variable thickness rotating discs.

Timoshenko and Goodier were the first to propose a closed-form set of stress equations for a rotating disk[36]. Gamer published four articles in the years 1983-1985, focusing on the deformation and stress distribution in rotating discs under different boundary conditions [37–40]. They based their

 doi:10.20944/preprints202401.1020.v1

analyses on the Tresca yield criterion and performed the flow law analysis. In Gamer's analyses, density and thickness were assumed to have constant distributions, [37] and they investigated the elastoplastic behavior in a rotating cylinder. Their analysis, based on the Tresca yield criterion, compared the stress distribution under two conditions: fully plastic and linear hardening.

Furthermore, the influence of density on the elastoplastic behavior of a hollow rotating disc with variable thickness was examined by Guven [41]. Guven then[42] analyzed an assumed disc under external pressure, focusing on angles corresponding to the yield threshold. Finally, Argso and his colleagues [43] investigated the velocity of homogenous variable-thickness discs.

Various research studies have been conducted on rotating disc and cylindrical structures made of functionally graded materials (FGM) due to the advantages they offer. Akis and Eraslan [44] investigated the yielding thresholds of hollow rotating shafts made of functionally graded materials using the Tresca yield criterion. They considered the elastic modulus and yield stress as power functions of the radial coordinate. Later, Argeso and Eraslan[45], based on the Tresca yield criterion, presented an exact solution for the elastoplastic analysis of a rotating functionally graded shaft.

Birman and Byrd [46] studied the stress in a functionally graded rotating disc, considering the Young's modulus and Poisson's ratio as power functions. They used the finite difference method for numerical analysis. Akis and Eraslan [47] performed an analytical elastoplastic analysis of a functionally graded rotating cylinder and utilized the ideal plasticity associated with the Tresca yield criterion for the plastic deformation analysis.

Bayat and his colleagues [48] analyzed a functionally graded rotating disc with variable thickness. They considered the material properties and disc profile as power functions along the radial direction. Madan and Saha [49] investigated the effect of functionally graded materials on the yield threshold of a thick-walled rotating cylinder. They also compared the yield criteria of von Mises and Tresca. Furthermore, they provided an exact solution for elastoplastic analysis of a thick-walled functionally graded rotating cylinder under pressure, considering the elastic modulus, density, and yield stress as power functions of the radial coordinates.

Ting-Dai and Hong-Dai[50]assumed a functionally graded hollow rotating disc with variable rotational velocity. They considered the elastic modulus and density of the rotating disc as variables along the radial direction. Ma and Hao [51] analyzed the elastoplastic deformation of a rotating disc beyond the yield limit. They examined the effects of various parameters, including cross-sectional profiles, and material properties on the critical velocitys of the disc. Peng and Li [52] analyzed the elastoplastic deformation of a rotating disc at velocitys exceeding the yield limit. They studied the effects of various parameters, including the cross-sectional profiles and material properties, on the critical velocitys of the disc. Additionally, they provided a numerical solution for the elastoplastic deformation of a functionally graded rotating disc, considering linear hardening.

Lomakin and his colleagues [53] analyzed the hollow rotating disc using the von Mises yield criterion along with the flow law to study the fields of stress and strain in the elastoplastic region.

The main objective of this research is to analyze the yielding threshold of a functionally graded hollow rotating disc with variable thickness. This analysis takes into account the variations in elastic modulus, density, and yield stress. The Tresca yield criterion is utilized to investigate the yielding conditions.

2. Equations of Motion

there is a hollow disk made of functionally graded materials, which is sufficiently thin and large, with inner radius a and outer radius b, rotating at an angular velocity ω. Considering the geometry of the problem, the formulation and analysis are performed in cylindrical coordinates (z, θ, r). The thickness of the disk section, elastic modulus, density, and yield stress are assumed to be power functions (1) of the radial coordinate:

Preprints (www.preprints.org) | NOT PEER-REVIEWED | Posted: 12 January 2024 doi:10.20944/preprints202401.1020.v1

$$h(r) = h_0\left(\frac{r}{b}\right)^{n_t}$$
$$E(r) = E_0\left(\frac{r}{b}\right)^{n_E}$$
$$\rho(r) = \rho_0\left(\frac{r}{b}\right)^{n_\rho}$$
$$\sigma_Y(r) = \sigma_{Y_0}\left(\frac{r}{b}\right)^{n_\sigma} \quad (1)$$

In order,h_0 the values of thickness, Young's modulus E_0 are given by equations (1). $\rho_0$density, and σ_{Y_0} yield stress at the outer radius $(r = b)$ are also provided. The parameters n_t,n_E,n_ρ and n_σ represent the geometric and material properties and are defined as per equations (2).

$$n_t = \delta_t n$$
$$n_E = \delta_E n$$
$$n_\rho = \delta_\rho n$$
$$n_\sigma = \delta_\sigma n \quad (2)$$

The values of δ_t , δ_E,δ_ρ and δ_σ are constant. If in equations (2), the material and geometric properties are represented in a general form as P, then the variation of p and its value at the outer radius with p_0 is shown dimensionless as $\bar{p} = p/p_0$. The results for the variation of material and geometric properties are depicted in Figure 1 for the dimensionless radius$\bar{r}$.

Preprints (www.preprints.org) | NOT PEER-REVIEWED | Posted: 12 January 2024 doi:10.20944/preprints202401.1020.v1

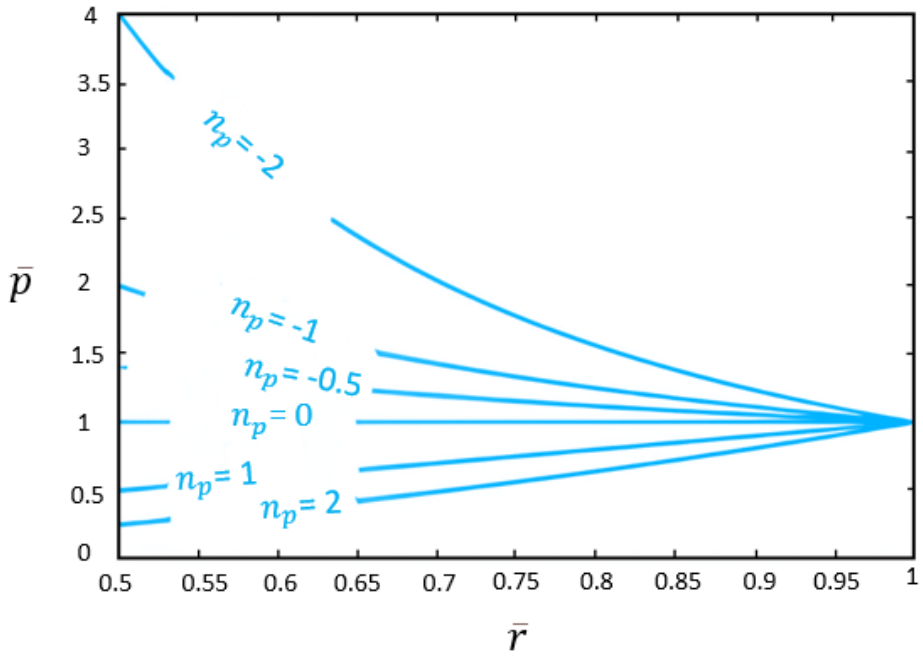

Figure 1. The graph of dimensional properties variations nondimensional radius $\bar{p}$ with respect to nondimensional radius $\bar{r}$.

The equation of motion for the rotating disk, considering the effect of thickness, is expressed as equation (3).

$$\frac{d}{dr}(hr\sigma_r) - h\sigma_\theta + h\rho\omega^2 r^2 = 0 \tag{3}$$

The components of radial and hoop stresses, σ_r and σ_θ, in equation (3) are represented. It should be noted that the volumetric force due to weight (ρg) has been neglected. Now, the radial and hoop displacements, u and v, are considered. Due to axial symmetry, there is no hoop displacement, and in other words, $v = 0$. Therefore, the stress equations in cylindrical coordinates are as follows:

$$\begin{aligned} \varepsilon_r &= \frac{du}{dr} \\ \varepsilon_\theta &= \frac{u}{r} \\ \gamma_{r\theta} &= 0 \end{aligned} \tag{4}$$

Using Hooke's law for the state of plane stress and displacement, strain equations (4) are employed, and the stress-displacement relationship is obtained in the form of equations (5).

Preprints (www.preprints.org) | NOT PEER-REVIEWED | Posted: 12 January 2024 doi:10.20944/preprints202401.1020.v1

$$\sigma_r = \frac{E(r)}{1-\nu^2}\left(\frac{du}{dr} + \nu\frac{u}{r}\right)$$
$$\sigma_\theta = \frac{E(r)}{1-\nu^2}\left(\frac{u}{r} + \nu\frac{du}{dr}\right) \quad (5)$$

By substituting the stress components into equation (3), the equation of motion the disk is transformed into the form of equation (6).

$$r^2\frac{d^2u}{dr^2} + (n_E + n_t + 1)r\frac{du}{dr} + ((n_E + n_t)\nu - 1)u = -\frac{1-\nu^2}{E_0}\rho_0 b^{n_E - n_\rho}\omega^2 r^{(n_\rho - n_E + 3)} \quad (6)$$

The analytical solution of the second-order differential equation (6) has a general solution in the form of equation (7):

$$u = -Ar^{m_3} + C_1 r^{m_1} + C_2 r^{m_2} \quad (7)$$

In which C_1 and C_2 are integration constants. Also, the constant parameters in equation (7) are defined as equations (8).

$$A = \frac{\left(\frac{1-\nu^2}{E_0}\right)\rho_0 b^{n_E - n_\rho}\omega^2}{n_\rho(n_\rho + 6) + (\nu - n_\rho - 3)n_E + (n_\rho - n_E + 3 + \nu)n_t + 8}$$
$$m_1 = \frac{-(n_E + n_t) + \sqrt{(n_E + n_t)^2 - 4((n_E + n_t)\nu - 1)}}{2}$$
$$m_2 = \frac{-(n_E + n_t) - \sqrt{(n_E + n_t)^2 - 4((n_E + n_t)\nu - 1)}}{2}$$
$$m_3 = n_\rho - n_E + 3 \quad (8)$$

Preprints (www.preprints.org) | NOT PEER-REVIEWED | Posted: 12 January 2024 doi:10.20944/preprints202401.1020.v1

By substituting the displacement equation (7) into the strain equations (5), the radial and hoop stresses are obtained in terms of the constants C_1 and C_2 as equations (9).

$$\sigma_r = \frac{E(r)}{1-\nu^2}[-A(m_3+\nu)r^{(m_3-1)}+(m_1+\nu)C_1 r^{m_1-1}+(m_2+\nu)C_2 r^{m_2-1}]$$

$$\sigma_\theta = \frac{E(r)}{1-\nu^2}[-A(m_3\nu+1)r^{m_3-1}+(m_1\nu+1)C_1 r^{m_1-1}+(m_2\nu+1)C_2 r^{m_2-1}] \quad (9)$$

The constants C_1 and C_2 are obtained. For a hollow disk, the radial stress at the inner boundaries $(\sigma_r)_{r=a}$ and the exterior $(\sigma_r)_{r=b}$ is zero. Therefore, by applying the boundary conditions for the disk, the constants C_1 and C_2 are obtained in equation (10).

$$C_1 = \frac{(a^{m_2}b^{(3)} - a^{m_3}b^{m_2+n_E-n_\rho})R}{(m_1+\nu)(a^{m_2}b^{m_1}-a^{m_1}b^{m_2})}$$
$$C_2 = \frac{(a^{m_3-1}b^{n_E-n_\rho+m_1-1} - a^{m_1-1}b^{(2)})R}{(m_2+\nu)(a^{m_2-1}b^{m_1-1}-a^{m_1-1}b^{m_2-1})} \quad (10)$$

In which R is a constant parameter defined in equation (10) as follows:

$$R = \frac{(m_3+\nu)\left(\frac{1-\nu^2}{E_0}\right)\rho_0\omega^2}{n_\rho(n_\rho+6)+(\nu-n_\rho-3)n_E+(n_\rho-n_E+3+\nu)n_t+8} \quad (11)$$

In order to obtain general solutions, the derived equations are made dimensionless using equations (12).

$$\bar{u} = \frac{uE_0}{\sigma_{Y_0}b}, \quad \Omega = \left(\frac{\rho}{\sigma_{Y_0}}\right)^{1/2} b\omega, \quad \bar{r} = \frac{r}{b}$$
$$\bar{\sigma}_r = \frac{\sigma_r}{\sigma_{Y_0}}, \quad \bar{\sigma}_\theta = \frac{\sigma_\theta}{\sigma_{Y_0}}, \quad \bar{a} = \frac{a}{b}$$
$$\bar{C}_1 = \frac{C_1E_0b^{m_1-1}}{\sigma_{Y_0}}, \quad \bar{C}_2 = \frac{C_2E_0b^{m_2-1}}{\sigma_{Y_0}} \quad (12)$$

3. Analyze yielding state

In order to determine the angular velocities corresponding to the yielding threshold and examine the yielding conditions, the Tresca yielding criterion has been employed. The utilization of the Tresca yielding criterion necessitates establishing the order of principal stresses σ_r and σ_θ. On the other hand, the order of principal stresses is dependent on the numerical values of the power parameters

Preprints (www.preprints.org) | NOT PEER-REVIEWED | Posted: 12 January 2024 doi:10.20944/preprints202401.1020.v1

(n_t, n_p,n_E and n_σ) and the ratio of radii (r/b). Therefore, for monitoring the initiation of yielding, a dimensionless variable Ψ based on the Tresca criterion is utilized. This variable is defined by the equation (13).

$$\Psi(\bar{r}) = \bar{r}^{(-n_\sigma)} Max\{(\bar{\sigma}_\theta - \bar{\sigma}_r), (\bar{\sigma}_\theta), (\bar{\sigma}_r)\} \tag{13}$$

The aforementioned criterion indicates that yielding initiates from points where $\Psi = 1$, and at the onset of yielding, the dimensionless function Ψ attains its maximum value.

For the analysis of the behavior of the rotating functionally graded material (FGM) disk, depending on the values of the power parameters, yielding may initiate from the inner radius, the outer radius, both simultaneously, or the intermediate region between the inner and outer radii.

3.1. State 1: Initiating yielding from the inner radius

Yielding occurs when $\Psi(\bar{a}) = 1$ and the function Ψ has its maximum absolute value at the inner radius. By utilizing the stress equations (9) and applying the boundary condition $(\bar{\sigma}_r)_{\bar{r}=\bar{a}=0}$, the dimensionless terminal rotational velocity Ω_{e1} can be defined as per the equation (14):

$$\begin{aligned}\Omega_{e1} = \{S[&-(m_1+\nu)(m_2+\nu)(m_3\nu+1)(\bar{a}^{m_2}-\bar{a}^{m_1})\bar{a}^{(m_3)} \\ &+(m_1\nu+1)(m_2+\nu)(m_3+\nu)(\bar{a}^{m_2}-\bar{a}^{m_3})\bar{a}^{m_1} \\ &+(m_2\nu+1)(m_1+\nu)(m_3+\nu)(\bar{a}^{m_3}-\bar{a}^{m_1})\bar{a}^{m_2}]^{-1}\}^{0.5}\end{aligned} \tag{14}$$

The constant S is defined as equation (15).

$$S = \frac{(1-\nu^2)(m_1+\nu)(m_2+\nu)(\bar{a}^{m_2}-\bar{a}^{m_1})}{H(\bar{a})^{n_E-n_\sigma-1}} \tag{15}$$

Where H is expressed as equation (16).

$$H = \frac{(1-\nu^2)}{n_\rho(n_\rho+6)+(\nu-n_\rho-3)n_E+(n_\rho-n_E+3+\nu)n_t+8} \tag{16}$$

3.2. State 2: Initiating yielding from the outer radius

In this case, yielding occurs when $\Psi(1) = 1$ and the function Ψ has its maximum absolute value at the outer radius. By using the stress equations (9) and applying the boundary condition $(\bar{\sigma}_r)_{\bar{r}=\bar{b}} = 0$, the dimensionless terminal rotational velocity ω_{e_2} is defined as an equation (17):

Preprints (www.preprints.org) | NOT PEER-REVIEWED | Posted: 12 January 2024 doi:10.20944/preprints202401.1020.v1

$$\Omega_{e2} = \{S_b[-(m_1+\nu)(m_2+\nu)(m_3\nu+1)(\bar{a}^{m_2}-\bar{a}^{m_1}) + (m_1\nu+1)(m_2+\nu)(m_3+\nu)(\bar{a}^{m_2}-\bar{a}^{m_3}) + (m_2\nu+1)(m_1+\nu)(m_3+\nu)(\bar{a}^{m_3}-\bar{a}^{m_1})]^{-1}\}^{0.5} \quad (17)$$

In which the constant S_b is defined as equation (18):

$$S_b = \frac{(1-\nu^2)(m_1+\nu)(m_2+\nu)(\bar{a}^{m_2}-\bar{a}^{m_1})}{H} \quad (18)$$

3.3. State 3: Simultaneous yielding initiation from both inner and outer radii.

In this case, yielding commences simultaneously from the inner and outer radii when both $\Psi(\bar{a}) = 1$ and $\Psi(1) = 1$ are satisfied, and the function Ψ must have maximum absolute values at both the inner and outer radii. Considering the boundary conditions of the disc and using equations (14) and(17), the critical dimensionless angular velocity ω_{c_r} and critical power parameter n_{c_r} can be obtained by solving the system of equations (19).

$$\begin{aligned}
&\Omega_{cr} - \{S_a[-(m_1+\nu)(m_2+\nu)(m_3\nu+1)(\bar{a}^{m_2}-\bar{a}^{m_1})\bar{a}^{(m_3)} \\
&+ (m_1\nu+1)(m_2+\nu)(m_3+\nu)(\bar{a}^{m_2}-\bar{a}^{m_3})\bar{a}^{m_1} \\
&+ (m_2\nu+1)(m_1+\nu)(m_3+\nu)(\bar{a}^{m_3}-\bar{a}^{m_1})\bar{a}^{m_2}]^{-1}\}^{0.5} = 0 \\
&\Omega_{cr} - \{S_b[-(m_1+\nu)(m_2+\nu)(m_3\nu+1)(\bar{a}^{m_2}-\bar{a}^{m_1}) \\
&+ (m_1\nu+1)(m_2+\nu)(m_3+\nu)(\bar{a}^{m_2}-\bar{a}^{m_3}) \\
&+ (m_2\nu+1)(m_1+\nu)(m_3+\nu)(\bar{a}^{m_3}-\bar{a}^{m_1})]^{-1}\}^{0.5} = 0
\end{aligned} \quad (19)$$

3.4. State 4: Yielding initiation from a radius between the inner and outer radii.

To initiate yielding from a radius between the inner and outer radii, the dimensionless function Ψ at the yielding initiation point r_{ep} must be equal to 1 and have the maximum absolute value at this point. For this reason, equation (20) must hold true to initiate yielding from the boundary between the inner and outer radii.

$$\begin{cases} \Psi(\bar{r}_{ep}) = 1 \\ \left.\dfrac{d\Psi}{dr}\right|_{\bar{r}=\bar{r}_{ep}} = 0 \end{cases} \quad (20)$$

 doi:10.20944/preprints202401.1020.v1

Equation (20) is used to calculate the required terminal rotational velocity for initiating plastic flow and the location of yielding initiation point $\bar{r}_{ep}$ for a specific power parameter n.

4. Conclusion

In this paper, an analytical study of the threshold of yielding in a variable thickness rotating disk made of functionally graded materials (FGM) based on the Tresca criterion is presented. The thickness of the disk cross-section, modulus of elasticity, density, and yield stress were assumed to be power functions of the radial coordinate. The effects of various parameters on the initiation of yielding in the rotating disk were investigated in this study. Furthermore, emphasizing that yielding always initiates from the inner radius in homogeneous rotating disks, different scenarios were considered for the initiation of yielding and the propagation of plastic flow in the target rotating disk. The results clearly demonstrate the significance of considering thickness variations in the analysis of the threshold of yielding in the target rotating disk.

For the results of this draft, please consider contacting the first author of this paper.

References

1. Tajdari, F.; Roncoli, C. Online set-point estimation for feedback-based traffic control applications. *IEEE Transactions on Intelligent Transportation Systems* **2023**.
2. Tajdari, F.; Ramezanian, H.; Paydarfar, S.; Lashgari, A.; Maghrebi, S. Flow metering and lane-changing optimal control with ramp-metering saturation. 2022 CPSSI 4th International Symposium on Real-Time and Embedded Systems and Technologies (RTEST). IEEE, 2022, pp. 1–6.
3. Rad, N.F.; Yousefi-Koma, A.; Tajdari, F.; Ayati, M. Design of a novel three degrees of freedom ankle prosthesis inspired by human anatomy. 2016 4th International Conference on Robotics and Mechatronics (ICROM). IEEE, 2016, pp. 428–432.
4. Rad, N.F.; Ayati, M.; Basaeri, H.; Yousefi-Koma, A.; Tajdari, F.; Jokar, M. Hysteresis modeling for a shape memory alloy actuator using adaptive neuro-fuzzy inference system. 2015 3Rd RSI international conference on robotics and mechatronics (ICROM). IEEE, 2015, pp. 320–324.
5. Tajdari, F.; Huysmans, T.; Song, Y. Non-rigid registration via intelligent adaptive feedback control. *IEEE transactions on visualization and computer graphics* **2023**.
6. Tajdari, M.; Tajdari, F.; Pawar, A.; Zhang, J.; Liu, W.K. 2d to 3d volumetric reconstruction of human spine for diagnosis and prognosis of spinal deformities. Conference: 16th US national congress on computational mechanics, 2021.
7. Tajdari, M.; Pawar, A.; Li, H.; Tajdari, F.; Maqsood, A.; Cleary, E.; Saha, S.; Zhang, Y.J.; Sarwark, J.F.; Liu, W.K. Image-based modelling for adolescent idiopathic scoliosis: mechanistic machine learning analysis and prediction. *Computer methods in applied mechanics and engineering* **2021**, *374*, 113590.
8. Tajdari, F.; Roncoli, C.; Papageorgiou, M. Feedback-based ramp metering and lane-changing control with connected and automated vehicles. *IEEE Transactions on Intelligent Transportation Systems* **2020**, *23*, 939–951.
9. Tajdari, F.; Roncoli, C.; Bekiaris-Liberis, N.; Papageorgiou, M. Integrated ramp metering and lane-changing feedback control at motorway bottlenecks. 2019 18th European Control Conference (ECC). IEEE, 2019, pp. 3179–3184.
10. Ghaffari, A.; Khodayari, A.; Kamali, A.; Tajdari, F.; Hosseinkhani, N. New fuzzy solution for determining anticipation and evaluation behavior during car-following maneuvers. *Proceedings of the Institution of Mechanical Engineers, Part D: Journal of automobile engineering* **2018**, *232*, 936–945.
11. Khodayari, A.; Ghaffari, A.; Kamali, A.; Tajdari, F. A new model of car following behavior based on lane change effects using anticipation and evaluation idea. *Iranian Journal of Mechanical Engineering Transactions of the ISME* **2015**, *16*, 26–38.
12. Tajdari, F.; Roncoli, C. Adaptive traffic control at motorway bottlenecks with time-varying fundamental diagram. *IFAC-PapersOnLine* **2021**, *54*, 271–277.
13. Tajdari, F.; Toulkani, N.E.; Zhilakzadeh, N. Intelligent optimal feed-back torque control of a 6dof surgical rotary robot. 2020 11th Power Electronics, Drive Systems, and Technologies Conference (PEDSTC). IEEE, 2020, pp. 1–6.

14. Tajdari, F.; Kabganian, M.; Rad, N.F.; Khodabakhshi, E. Robust control of a 3-dof parallel cable robot using an adaptive neuro-fuzzy inference system. 2017 Artificial Intelligence and Robotics (IRANOPEN). IEEE, 2017, pp. 97–101.
15. Tajdari, F.; Kabganian, M.; Khodabakhshi, E.; Golgouneh, A. Design, implementation and control of a two-link fully-actuated robot capable of online identification of unknown dynamical parameters using adaptive sliding mode controller. 2017 Artificial Intelligence and Robotics (IRANOPEN). IEEE, 2017, pp. 91–96.
16. Saleh, B.; Jiang, J.; Fathi, R.; Al-hababi, T.; Xu, Q.; Wang, L.; Song, D.; Ma, A. 30 Years of functionally graded materials: An overview of manufacturing methods, Applications and Future Challenges. *Composites Part B: Engineering* **2020**, *201*, 108376.
17. Tajdari, F.; Toulkani, N.E.; Zhilakzadeh, N. Semi-real evaluation, and adaptive control of a 6dof surgical robot. 2020 11th Power Electronics, Drive Systems, and Technologies Conference (PEDSTC). IEEE, 2020, pp. 1–6.
18. Tajdari, F.; Tajdari, M.; Rezaei, A. Discrete time delay feedback control of stewart platform with intelligent optimizer weight tuner. 2021 IEEE International Conference on Robotics and Automation (ICRA). IEEE, 2021, pp. 12701–12707.
19. Tajdari, F.; Ebrahimi Toulkani, N. Implementation and intelligent gain tuning feedback–based optimal torque control of a rotary parallel robot. *Journal of Vibration and Control* **2022**, *28*, 2678–2695.
20. Tajdari, F. Adaptive time-delay estimation and control of optimized stewart robot. *Journal of Vibration and Control* **2023**, *29*, 5511–5531.
21. Tajdari, F.a. Advancing non-rigid 3D/4D human mesh registration for ultra-personalization **2023**.
22. Tajdari, F.; Khodabakhshi, E.; Kabganian, M.; Golgouneh, A. Switching controller design to swing-up a two-link underactuated robot. 2017 IEEE 4th International Conference on Knowledge-Based Engineering and Innovation (KBEI). IEEE, 2017, pp. 0595–0599.
23. Tajdari, F.; Huysmans, T.; Yang, Y.; Song, Y. Feature preserving non-rigid iterative weighted closest point and semi-curvature registration. *IEEE Transactions on Image Processing* **2022**, *31*, 1841–1856.
24. Tajdari, F.; Ghaffari, A.; Khodayari, A.; Kamali, A.; Zhilakzadeh, N.; Ebrahimi, N. Fuzzy control of anticipation and evaluation behaviour in real traffic flow. 2019 7th International Conference on Robotics and Mechatronics (ICRoM). IEEE, 2019, pp. 248–253.
25. Yang, Y.; Yuan, T.; Huysmans, T.; Elkhuizen, W.S.; Tajdari, F.; Song, Y. Posture-invariant three dimensional human hand statistical shape model. *Journal of Computing and Information Science in Engineering* **2021**, *21*, 031006.
26. Tajdari, F.; Kwa, F.; Versteegh, C.; Huysmans, T.; Song, Y. Dynamic 3d mesh reconstruction based on nonrigid iterative closest-farthest points registration. International design engineering technical conferences and computers and information in engineering conference. American Society of Mechanical Engineers, 2022, Vol. 86212, p. V002T02A051.
27. Tajdari, F.; Golgouneh, A.; Ghaffari, A.; Khodayari, A.; Kamali, A.; Hosseinkhani, N. Simultaneous intelligent anticipation and control of follower vehicle observing exiting lane changer. *IEEE Transactions on Vehicular Technology* **2021**, *70*, 8567–8577.
28. Tajdari, F.; Eijck, C.; Kwa, F.; Versteegh, C.; Huysmans, T.; Song, Y. Optimal position of cameras design in a 4d foot scanner. International design engineering technical conferences and computers and information in engineering conference. American Society of Mechanical Engineers, 2022, Vol. 86212, p. V002T02A044.
29. Tajdari, M.; Tajdari, F.; Shirzadian, P.; Pawar, A.; Wardak, M.; Saha, S.; Park, C.; Huysmans, T.; Song, Y.; Zhang, Y.J.; others. Next-generation prognosis framework for pediatric spinal deformities using bio-informed deep learning networks. *Engineering with Computers* **2022**, *38*, 4061–4084.
30. Tajdari, F.; Huysmans, T.; Yao, X.; Xu, J.; Song, Y. 4D Feet: Registering Walking Foot Shapes Using Attention Enhanced Dynamic-Synchronized Graph Convolutional LSTM Network. *arXiv preprint arXiv:2307.12377* **2023**.
31. Tajdari, F.; others. Optimal and adaptive controller design for motorway traffic with connected and automated vehicles **2023**.

32. Tarvirdizadeh, B.; Golgouneh, A.; Khodabakhshi, E.; Tajdari, F. An assessment of a similarity between the right and left hand photoplethysmography signals, using time and frequency features of heart-rate-variability signal. 2017 IEEE 4th international conference on knowledge-based engineering and innovation (KBEI). IEEE, 2017, pp. 0588–0594.
33. Tarvirdizadeh, B.; Golgouneh, A.; Tajdari, F.; Khodabakhshi, E. A novel online method for identifying motion artifact and photoplethysmography signal reconstruction using artificial neural networks and adaptive neuro-fuzzy inference system. *Neural Computing and Applications* **2020**, *32*, 3549–3566.
34. Golgouneh, A.; Bamshad, A.; Tarvirdizadeh, B.; Tajdari, F. Design of a new, light and portable mechanism for knee CPM machine with a user-friendly interface. 2016 Artificial Intelligence and Robotics (IRANOPEN). IEEE, 2016, pp. 103–108.
35. Minnoye, A.L.; Tajdari, F.; Doubrovski, E.L.; Wu, J.; Kwa, F.; Elkhuizen, W.S.; Huysmans, T.; Song, Y. Personalized product design through digital fabrication. International Design Engineering Technical Conferences and Computers and Information in Engineering Conference. American Society of Mechanical Engineers, 2022, Vol. 86212, p. V002T02A054.
36. Timoshenko, S.; Goodier, J. Theory of Elasticity, modulus, 1969.
37. Gamer, U.; Lance, R.H. Stress distribution in a rotating elastic-plastic tube. *Acta Mechanica* **1983**, *50*, 1–8.
38. Gamer, U.a. The elastic-plastic stress-distribution in the rotating annulus and in the annulus under external-pressure. *ZAMM* **1984**, *64*, T126–T128.
39. Gamer, U. Elastic-plastic deformation of the rotating solid disk. *Archive of Applied Mechanics* **1984**, *54*, 345–354.
40. Gamer, U.a. Stress distribution in the rotating elastic-plastic disk. *Zamm* **1985**, *65*, 136–137.
41. Güven, U. Elastic-plastic stresses in a rotating annular disk of variable thickness and variable density. *International Journal of Mechanical Sciences* **1992**, *34*, 133–138.
42. Guven, U. On the stresses in an elastic-plastic annular disk of variable thickness under external pressure. *International Journal of Solids and Structures* **1993**, *30*, 651–658.
43. Eraslan, A.N.; Argeso, H. Limit angular velocities of variable thickness rotating disks. *International Journal of Solids and Structures* **2002**, *39*, 3109–3130.
44. Akis, T.; Eraslan, A.N. The stress response and onset of yield of rotating FGM hollow shafts. *Acta Mechanica* **2006**, *187*, 169–187.
45. Argeso, H.; Eraslan, A.N. A computational study on functionally graded rotating solid shafts. *International Journal for Computational Methods in Engineering Science and Mechanics* **2007**, *8*, 391–399.
46. Birman, V.; Byrd, L.W. Modeling and analysis of functionally graded materials and structures **2007**.
47. Akis, T.; Eraslan, A.N. Exact solution of rotating FGM shaft problem in the elastoplastic state of stress. *Archive of Applied Mechanics* **2007**, *77*, 745–765.
48. Bayat, M.; Saleem, M.; Sahari, B.; Hamouda, A.; Mahdi, E. Analysis of functionally graded rotating disks with variable thickness. *Mechanics Research Communications* **2008**, *35*, 283–309.
49. Madan, R.; Saha, K.; Bhowmick, S. Limit speeds and stresses in power law functionally graded rotating disks. *Advances in materials Research* **2020**, *9*, 115–131.
50. Dai, T.; Dai, H.L. Investigation of mechanical behavior for a rotating FGM circular disk with a variable angular speed. *Journal of Mechanical Science and Technology* **2015**, *29*, 3779–3787.
51. Ma, G.; Hao, H.; Miyamoto, Y. Limit angular velocity of rotating disc with unified yield criterion. *International journal of mechanical sciences* **2001**, *43*, 1137–1153.
52. Peng, X.L.; Li, X.F. Effects of gradient on stress distribution in rotating functionally graded solid disks. *Journal of Mechanical Science and Technology* **2012**, *26*, 1483–1492.
53. Lomakin, E.; Alexandrov, S.; Jeng, Y.R. Stress and strain fields in rotating elastic/plastic annular discs. *Archive of Applied Mechanics* **2016**, *86*, 235–244.